Supporting Information

Plasmonic and nanozyme dual channel-based logic judgment for enhancing gold nanoparticles colorimetric Hg^{2+} ions performance

Kehui Zhang,[a] Mingyue Luo,[a] Honghong Rao,[b] Haile Liu,[a] Ruibin Qiang,[a] Xin Xue,[c] Jianying Li,[a] Xiaoquan Lu[a] and Zhonghua Xue[a]*

[a] Key Laboratory of Water Security and Water Environment Protection in Plateau Intersection (NWNU), Ministry of Education; Key Lab of Bioelectrochemistry and Environmental Analysis of Gansu Province, College of Chemistry and Chemical Engineering, Northwest Normal University, Lanzhou, 730070 (China)

[b] School of Chemical Engineering, Lanzhou City University, Lanzhou, 730070 (China)

[c] State Key Laboratory of Applied Organic Chemistry and Key Laboratory of Nonferrous Metal Chemistry and Resources Utilization of Gansu Province, Lanzhou University, Lanzhou, 730000 (China)
E-mail address: xzhlab@hotmail.com (Z. H. Xue).

Materials and regents

The chemical reagents used in the experiments were all of analytical grade. The water used in all the experiments was obtained from the Ulupure UPT-II system (18.24 MΩ·cm). $HAuCl_4·4H_2O$ was provided by Sigma-Aldrich. The mercury ion (Hg^{2+}) standard solutions were purchased from Guobiao (Beijing) Testing & Certification Co., Ltd. Trisodium citrate, 3,3′,5,5′-tetramethylbenzidine (TMB), hydrogen peroxide (H_2O_2), tris(hydroxymethyl)aminomethane (Tris), hydrochloric acid (HCl), and related inorganic salts (NaCl, KCl, $AgNO_3$, $Ni(NO_3)_2$, $Zn(NO_3)_2$, $MgCl_2$, $MnCl_2$, $CoCl_2$, $BaSO_4$, $Cu(NO_3)_2$, $Cd(NO_3)_2$, $Pb(NO_3)_2$, $Fe(NO_3)_3$, $FeCl_2$, $Ce(NO_3)_3$, $Bi(NO_3)_3$, $CrCl_3$, $AlCl_3$, NaF, NaBr, NaI, $NaAsO_2$, Na_3AsO_4, Na_3PO_4, Na_2SO_4, Na_2S, Na_2SO_3, $Hg(NO_3)_2$) were purchased from Sinopharm Chemical Reagent. Dopamine, melamine, and kanamycin were purchased from Shanghai Aladdin Biochemical Technology Co., Ltd. The DNA oligonucleotide was synthesized by Sangon Biotech (Shanghai) Co., Ltd., and the sequence was 5′-TTCTTTCTTCCCCTTGTTTGTT-3′, according to the previously reported literature.[1] And the DNA oligonucleotide solution was prepared with 0.02 M Tris-HCl buffer (pH 7.4) containing 0.1 M NaCl and 5 mM KCl.

Instrumentation

Ultraviolet-visible (UV-vis) absorption spectra were measured by a T6 new century UV-vis spectrophotometer. Transmission electron microscopy (TEM) images were measured by an FEI Tecnai G2 F20 STwin. X-ray photoelectron spectroscopy (XPS) was obtained by an ESCALAB 250Xi (Thermo Fisher Scientific, USA). Dynamic light scattering (DLS) was recorded by a Zetasizer Nano ZS ZEN3600 system (Malvern Instruments, UK).

Synthesis of AuNPs.

The AuNPs were synthesized according to the literature previously reported.[2] Specifically, 45 mL

of ultrahigh purity water, 2.5 mL of $HAuCl_4 \cdot 4H_2O$ (5×10^{-3} M), and 2.5 mL of trisodium citrate (1.7×10^{-2} M) were added to a 100 mL round-bottom flask equipped with a condenser. Subsequently, the mixed solution was heated to reflux at 100°C for 10 min, and it could be observed that the color of the mixed solution changed from light-yellow to wine-red indicating that AuNPs had been formed in the solution. Finally, the mixed solution was naturally cooled to room temperature, and obtain the AuNPs products.

Optimization of Hg^{2+} ions detection conditions.

To achieve optimal plasmonic and nanozyme dual-channel response signals for Hg^{2+} ions colorimetric analysis, some key testing conditions were optimized including the concentration of ssDNA and working buffer (i.e., salt-containing Tris-HCl buffer), the catalytic reaction time as well as the concentrations of the enzyme substrate of TMB and H_2O_2. For the AuNPs plasmonic response-related conditions, we referred to the previously reported incubation time, and optimized the concentration of ssDNA and the concentration of the working buffer using the $\Delta A_{650}/A_{530}$ (change in absorbance ratio at 650 nm to 530 nm before and after the Hg^{2+} ions addition). As shown in Fig. S4, the $\Delta A_{650}/A_{530}$ increased with the increasing ssDNA concentration, and reached equilibrium at a concentration of 42 nM. Similarly, it showed an increasing trend and then decreased with the increase of the working buffer concentration, and reached a maximum value at a concentration of 30 μL/mL (Fig. S5).

Subsequently, the reaction conditions related to the AuNPs nanozyme response including the catalytic reaction time, the concentration of ssDNA, working buffer as well as TMB and H_2O_2 were optimized by using the ΔA_{652} (change in absorbance at 652 nm before and after the Hg^{2+} ions addition). As shown in Fig. S6, the obtained ΔA_{652} increased with the increase of reaction time, and reached equilibrium at a reaction time of 7 min. It also increased with the increasing ssDNA concentration, and reached equilibrium at a concentration of 42 nM (Fig. S7). However, for the optimization of the working

buffer concentration, the obtained ΔA_{652} decreased with the increasing working buffer concentration (Fig. S8), which might be attributed to the more pronounced aggregation of gold amalgam at higher working buffer concentration, resulting in a reduced specific surface area and weakened peroxidase-like activity of AuNPs. Certainly, considering the fact that the working buffer with too low a concentration was unfavorable for AuNPs aggregation and their corresponding plasmonic signal responses, we thus used a working buffer concentration of 30 μL/mL as the optimal reaction condition for investigating AuNPs nanozyme response. As far as the optimization of TMB and H_2O_2 concentration, we found that ΔA_{652} increased with the increasing TMB concentration and reached equilibrium at a concentration of 1 mM (Fig. S9). However, it showed an increasing and then decreasing trend with the increasing H_2O_2 concentration and reached a maximum value at 30 mM (Fig. S10). In short, the ssDNA concentration of 42 nM, the working buffer concentration of 30 μL/mL, the catalytic reaction time of 7 min, the TMB concentration of 1 mM, and the H_2O_2 concentration of 30 mM were proposed as the optimal conditions to investigate AuNPs plasmonic and nanozyme response signals in our AuNPs colorimetric sensing system.

The above experiments were conducted in three sets of repetitive parallel experiments, and the data presented are the mean and standard deviation of the absorbance values measured in the three sets of experiments.

Colorimetric detection of Hg^{2+} ions based on AuNPs dual-channel response.

For the colorimetric assay, briefly, 10 μL of ssDNA (2.1 μM), 20 μL of different concentrations of Hg^{2+} ions, and 300 μL of AuNPs were first mixed and incubated for 30 min. Subsequently, 30 μL of working buffer solution (A 0.02 M Tris-HCl buffer (pH 7.4) containing 0.1 M NaCl and 5 mM KCl) was added to the mixed solution and incubated for 1 min. The changes in solution color and Vis-NIR spectra

produced by the AuNPs plasmonic response were recorded using a digital camera and a UV-Vis spectrophotometer.

In addition, since the working buffer solution contained both salt components (NaCl and KCl) and had a pH of 7.4, it not only induced aggregation of AuNPs, but also provided a suitable neutral environment for the next step of catalyzing enzyme substrates by AuNPs. Based on this, continue adding 20 μL of H_2O_2 (0.75 M) and 20 μL of TMB (25 mM) to the mixed solution and dilute to 500 μL reaction for 7 min. The changes in solution color and Vis-NIR spectra produced by the AuNPs nanozyme response were continued recorded using a digital camera and a UV-Vis spectrophotometer.

Following the same procedure as above, various interferents (Ag^+, Ni^{2+}, Zn^{2+}, Mg^{2+}, Mn^{2+}, Co^{2+}, Ba^{2+}, Cu^{2+}, Cd^{2+}, Pb^{2+}, Fe^{2+}, Fe^{3+}, Ce^{3+}, Bi^{3+}, Cr^{3+}, Al^{3+}, F^-, Br^-, I^-, AsO_2^-, $HAsO_4^{2-}$, PO_4^{2-}, SO_4^{2-}, S^{2-}, SO_3^{2-}, dopamine, melamine, and kanamycin) were chosen to verify the dual-channel recognition of Hg^{2+} ions.

The above experiments were conducted in three sets of repetitive parallel experiments, and the data presented are the mean and standard deviation of the absorbance values measured in the three sets of experiments.

Colorimetric detection of Hg^{2+} ions in real water samples.

The practicality of the method was verified by using tap water, Yellow River water and lake water as real water samples. The three collected samples were first filtered twice through a 0.22 μm microfiltration membrane. Subsequently, different concentrations of Hg^{2+} ions were spiked to the filtered real water samples. Finally, the recoveries of spiked Hg^{2+} ions in the three samples were determined by our proposed method and the inductively coupled plasma mass spectrometry (ICP-MS).

Since Hg^{2+} ions content (less than 5 nM) in these real samples was below the LOD of the proposed

colorimetric strategy, we therefore determined Hg^{2+} ions by using the standard addition method. Meanwhile, ICP-MS was also employed to verify the accuracy of the proposed method. Table S1 displays the average detection results, recoveries and relative standard deviations of target Hg^{2+} ions in three different real water samples that providing by the proposed method and ICP-MS, respectively. The recoveries of Hg^{2+} ions in tap water, Yellow River water, and lake water by our proposed method were 93.1 ~ 108.8%, 98.0 ~ 103.2%, and 95.6 ~ 105.7%, respectively, which were comparable to that of ICP-MS (99.1 ~ 106.1%). These results strongly demonstrated that the proposed method had good applicability and accuracy for Hg^{2+} ions detection in real water samples.

The above experiments were conducted in three sets of repetitive parallel experiments, and the data presented are the mean and standard deviation of the absorbance values measured in the three sets of experiments.

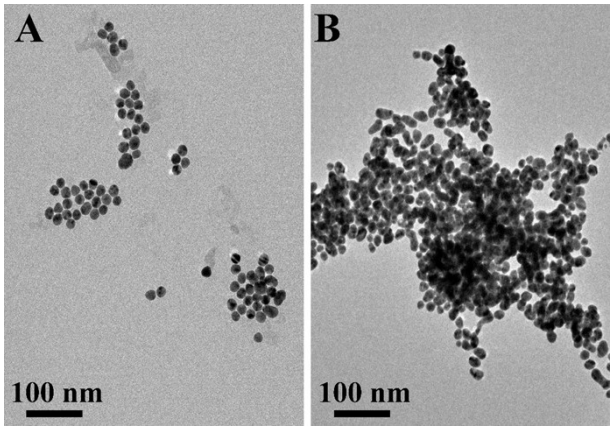

Fig. S1 TEM images of different components ((A) AuNPs + ssDNA + NaCl; (B) AuNPs + ssDNA + Hg^{2+} + NaCl).

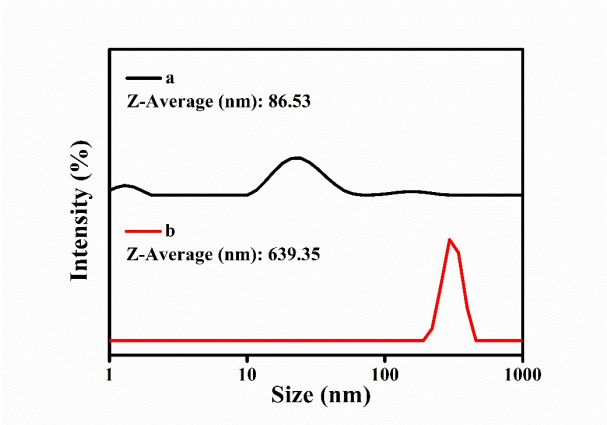

Fig. S2 DLS data of different components (a: AuNPs + ssDNA + NaCl; b: AuNPs + ssDNA + Hg^{2+} + NaCl).

DLS measurements (Fig. S1) revealed that the Z-average size of AuNPs nanoprobe after NaCl addition in the presence of Hg^{2+} ions (639.35 nm) is much larger than that in the absence of Hg^{2+} ions (86.53 nm), suggesting a significant Hg^{2+} ions-induced AuNPs aggregation.

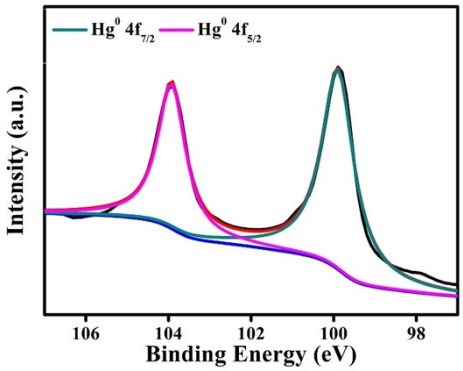

Fig. S3 The core-level Hg 4f XPS profile of the surface of AuNPs in the aptamer adsorption-based sensing system with added Hg^{2+} ions.

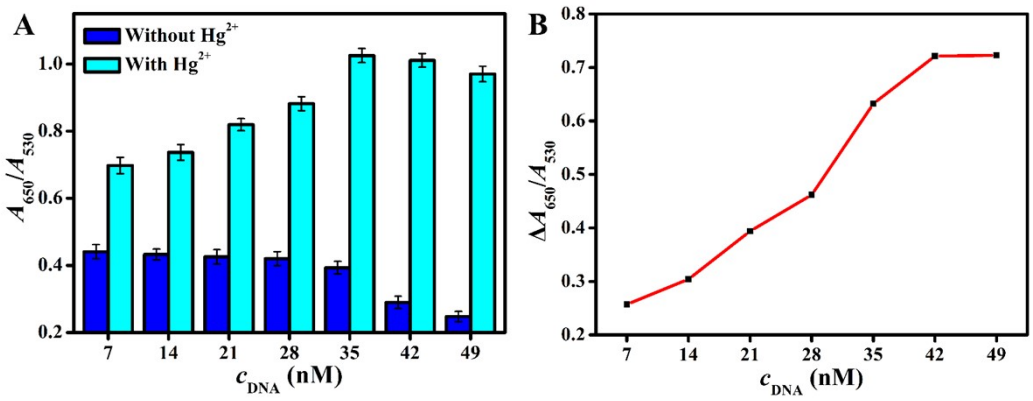

Fig. S4 Effects of DNA concentration on the plasmonic response of AuNPs to Hg^{2+} ions.

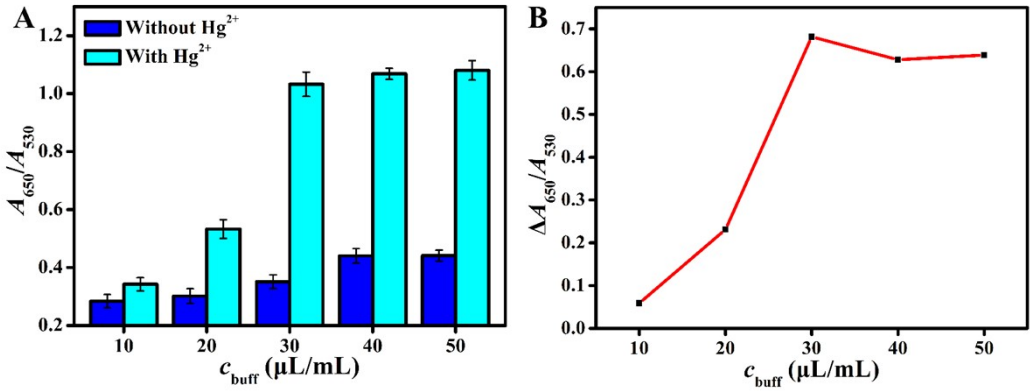

Fig. S5 Effects of working buff concentration on the plasmonic response of AuNPs to Hg^{2+} ions.

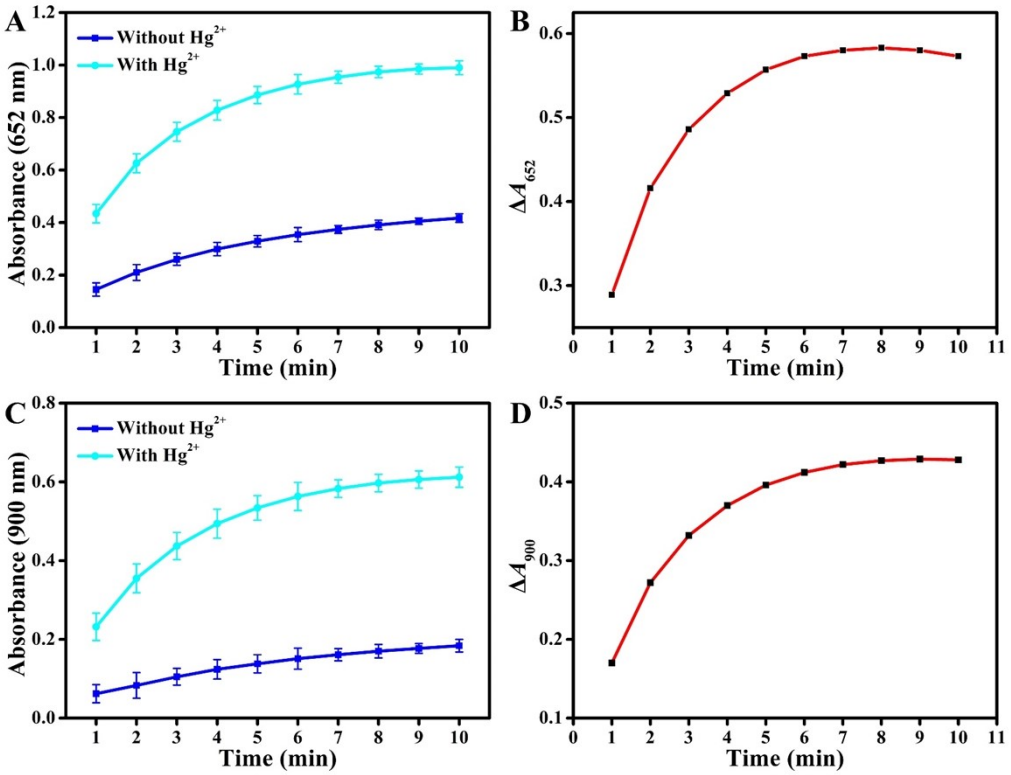

Fig. S6 Effects of reaction time on the nanozyme response of AuNPs to Hg^{2+} ions. (Fig. S4A and B show the results of reaction time optimization based on the absorbance value at 652 nm; Fig. S4C and D show the results of reaction time optimization based on the absorbance value at 900 nm.)

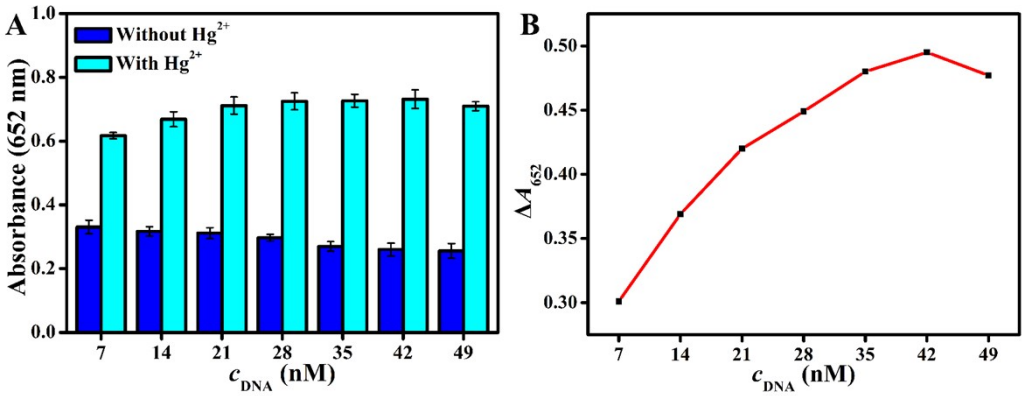

Fig. S7 Effects of DNA concentration on the nanozyme response of AuNPs to Hg^{2+} ions.

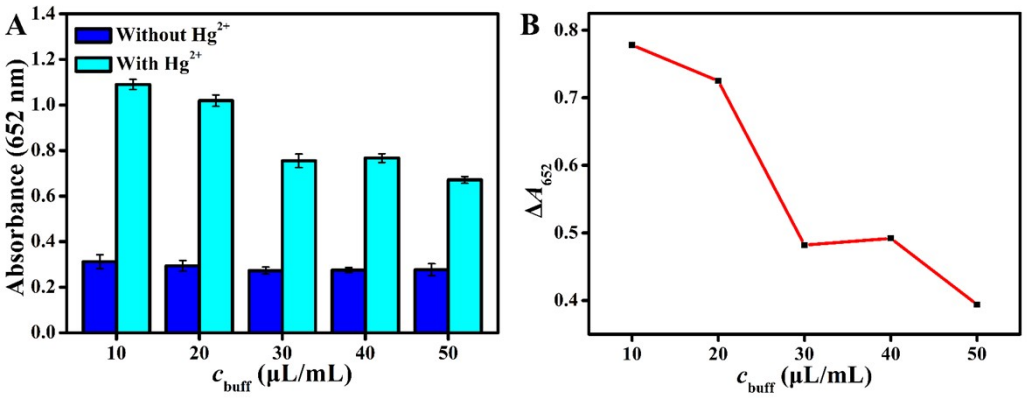

Fig. S8 Effects of working buff concentration on the nanozyme response of AuNPs to Hg^{2+} ions.

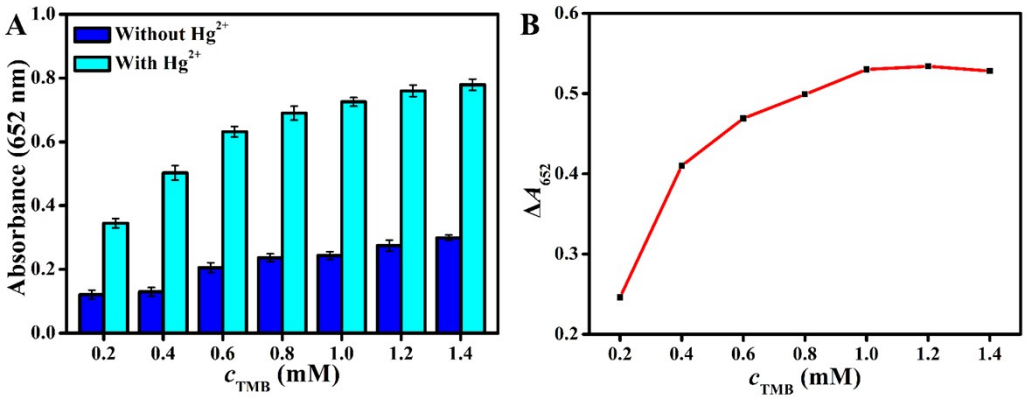

Fig. S9 Effects of TMB concentration on the nanozyme response of AuNPs to Hg^{2+} ions.

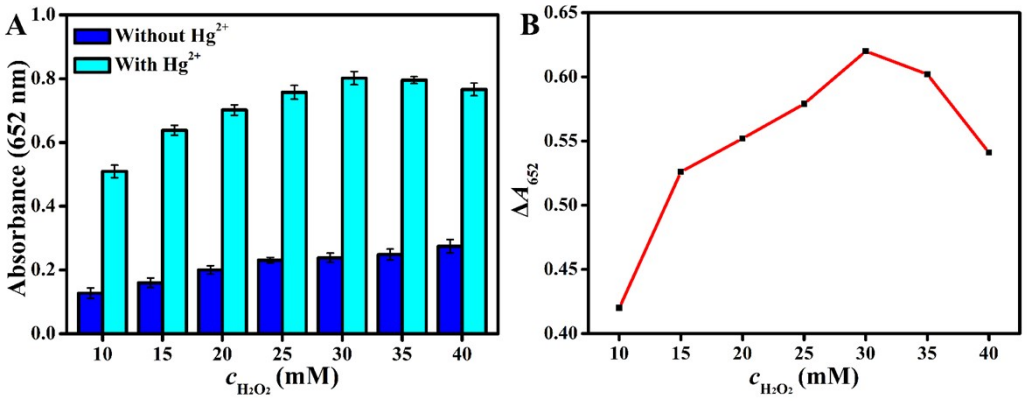

Fig. S10 Effects of H_2O_2 concentration on the nanozyme response of AuNPs to Hg^{2+} ions.

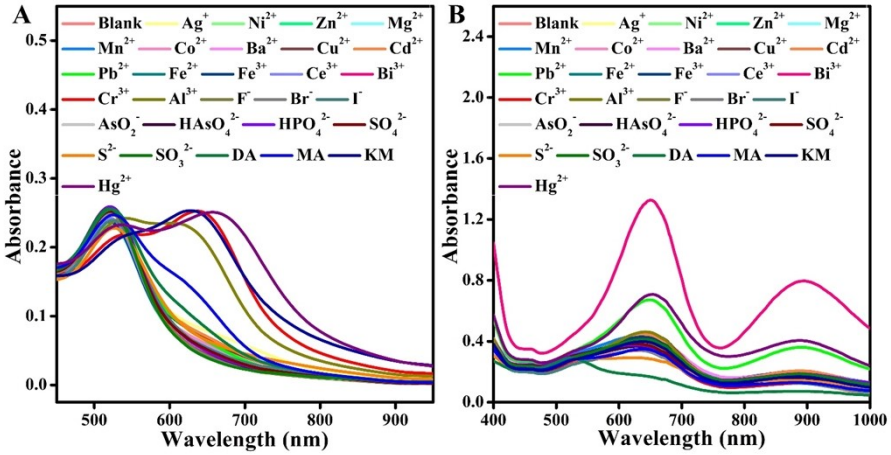

Fig. S11 The corresponding Vis-NIR absorption spectra of different interferents associated with the plasmonic (A) and nanozyme (B) response of AuNPs.

A

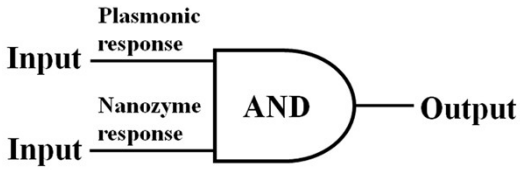

B

Input		Output	Judgment
Plasmonic response	Nanozyme response		
0	0	0	No target
1	0	0	Interferents
0	1	0	Interferents
1	1	1	Target

Fig. S12 Schematic illustration of AuNPs dual-channel response-based logic judgment for Hg^{2+} detection.

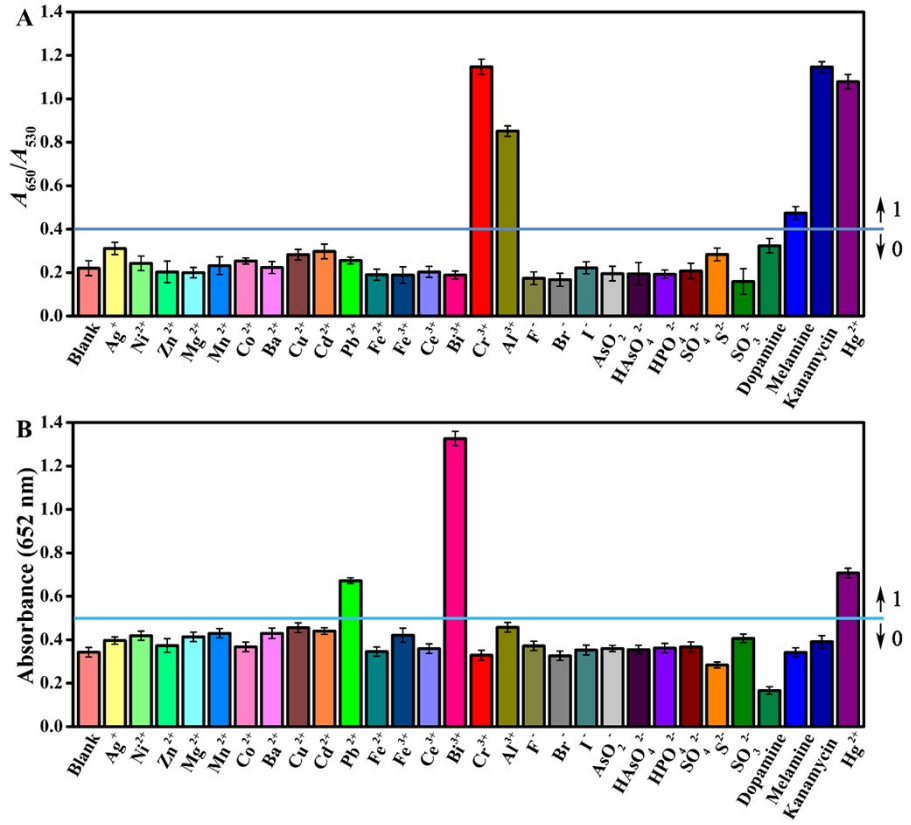

Fig. S13 (A) The A_{650}/A_{530} value of different interferents associated with the plasmonic response of AuNPs. (B) The A_{652} value of different interferents associated with the nanozyme response of AuNPs.

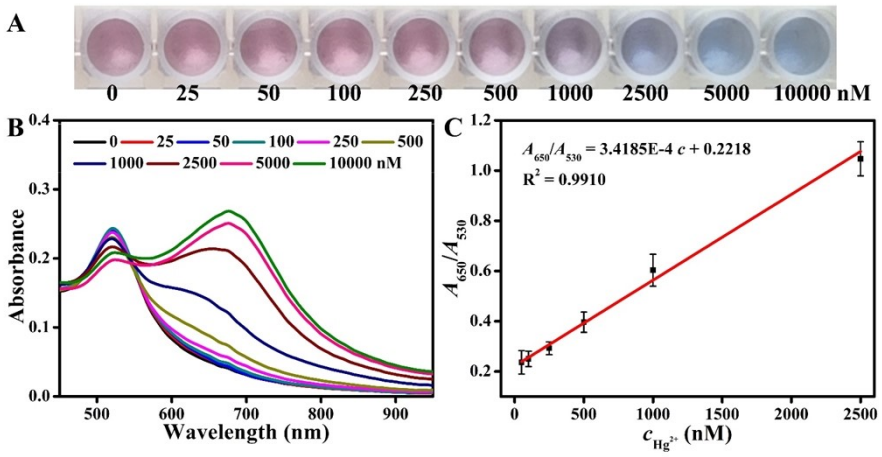

Fig. S14 Colors (A) and Vis-NIR absorption spectra (B) of reaction solutions with different Hg^{2+} concentrations in AuNP plasmonic response systems. (C) Linear relationship between A_{650}/A_{530} and Hg^{2+} concentration in the AuNP plasmonic response system.

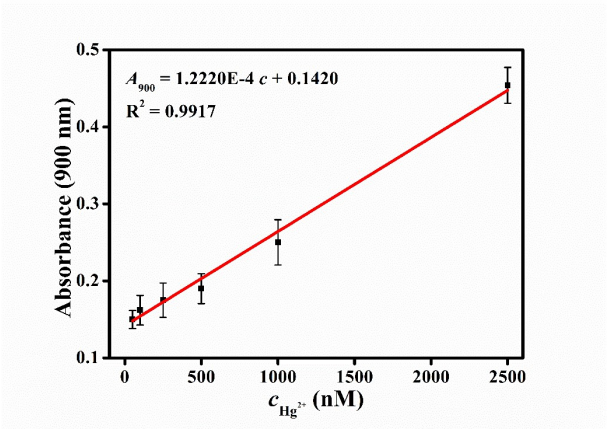

Fig. S15 Linear relationship between A_{900} and different concentrations of Hg^{2+} ions.

As shown in Fig. S11, Hg^{2+} ions showed a good linear relationship with A_{900} over the concentration range of 25 to 2500 nM. The obtained linear equation was A_{900} = 1.2220E−4 c + 0.1420 (R^2 = 0.9917), and the calculated LOD was 32.7 nM (S/N = 3). It could be seen that when the calibration curve was plotted using only the nanozyme response of the AuNPs (i.e., calibration curve based on absorbance at 900 nm), the sensitivity was still lower than that of the calibration curve integrating plasmonic and nanozyme dual responses of the AuNPs (i.e., calibration curve based on absorbance at 652 nm). Therefore, plotting the calibration curve by absorbance at 650 could obtain higher detection sensitivity.

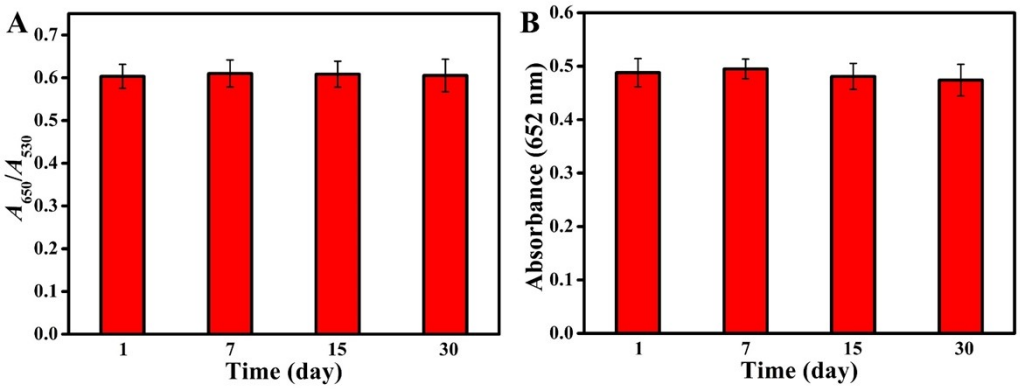

Fig. S16 Plasmonic (A) and nanozyme (B) response signal of the proposed method to Hg^{2+} ions at a concentration of 1000 nM over 7, 15, and 30 days.

During the 30-day experimental period, our proposed method found no significant changes in the plasmonic and nanozyme response signal of AuNPs to Hg^{2+} ions. It is shown that our proposed method has good stability and reproducibility.

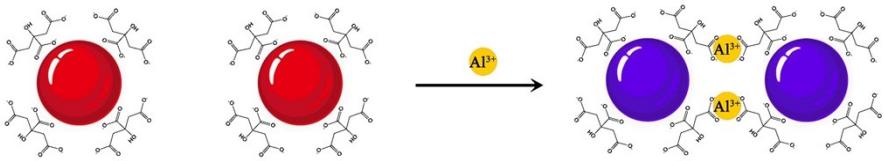

Fig. S17 Schematic representation of Al^{3+} ions-induced aggregation of citrate ligand-modified AuNPs.

Al^{3+} ions have a strong ability to bond with carboxyl groups. Thus, when citrate-modified AuNPs are used as probes, Al^{3+} ions can bind to the citrate ligand on the surface of the AuNPs, and further bridge adjacent AuNPs to cause aggregation of the particles.[3, 4]

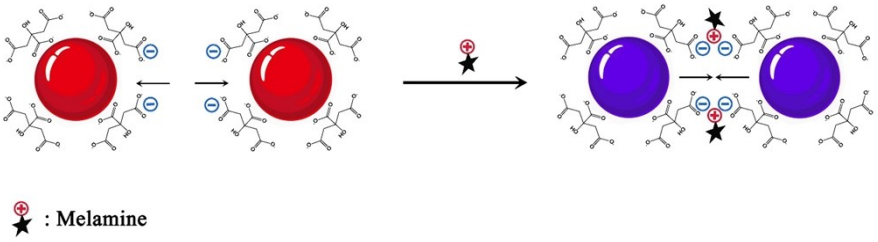

Fig. S18 (A) The A_{650}/A_{530} value of different interferents associated with the plasmonic response of AuNPs. (B) The A_{652} value of different interferents associated with the nanozyme response of AuNPs.

Citrate ligands are usually negatively charged, which provides a strong electrostatic repulsion between the AuNPs, allowing them to maintain a stable dispersion. However, positively charged melamine can affect the electrostatic repulsion between AuNPs through electrostatic interaction with the citrate ligand, leading to the aggregation of AuNPs.[5, 6]

Table S1. Detection of Hg^{2+} ions in real water samples.

Sample	Method	Spiked value (nM)	Found value (nM)	Recovery (%)	RSD (%, n = 3)
Tap water	Dual-channel mrthod	250	272.1	108.8	1.5
		500	497.9	99.5	2.1
		1000	931.1	93.1	1.2
	ICP-MS	250	265.3	106.1	2.1
		500	514.7	102.9	1.3
		1000	1022.4	102.2	1.7
Yellow River water	Dual-channel mrthod	250	247.7	99.1	1.7
		500	516.2	103.2	3.9
		1000	979.9	98.0	3.7
	ICP-MS	250	243.1	99.1	1.1
		500	528.6	105.7	0.9
		1000	1014.3	101.4	1.8
Lake water	Dual-channel mrthod	250	241.6	96.6	2.8
		500	528.4	105.7	3.3
		1000	955.5	95.6	1.3
	ICP-MS	250	260.4	104.1	2.4
		500	524.3	104.9	2.1
		1000	1018.6	101.9	1.8

Table S2 Comparison of the sening performance of different AuNPs-based colorimetric methods in Hg^{2+} assays.

Detection Methods	Material	Linear Range (M)	LOD (M)	Ref.
Colorimetric	Tween 20-AuNPs	$2.0 \times 10^{-7} – 8.0 \times 10^{-7}$	2×10^{-7}	[7]
Colorimetric	ssDNA-AuNPs	$9.6 \times 10^{-8} – 6.4 \times 10^{-6}$	4.0×10^{-8}	[1]
Colorimetric	DNA-AuNPs	$1.0 \times 10^{-7} – 2.0 \times 10^{-6}$	1.0×10^{-7}	[8]
Colorimetric	AuNPs@β-CD	$4.0 \times 10^{-7} – 8.0 \times 10^{-6}$	6.0×10^{-8}	[9]
Colorimetric	8-HQ-AuNPs	$1.0 \times 10^{-8} – 1.0\times 10^{-5}$	1.0×10^{-8}	[10]
Colorimetric	SnTe/Au	$2.0 \times 10^{-7} – 5.8\times 10^{-5}$	1.5×10^{-7}	[11]
Colorimetric	ssDNA-AuNPs	$2.5 \times 10^{-8} – 2.5\times 10^{-6}$	9.7×10^{-9}	This work

As shown in the Table S2, we listed some existing AuNPs-based colorimetric methods. In comparison, our proposed method has higher sensitivity and wider detection range for Hg^{2+} ions detection. More importantly, the LOD of our proposed method can reach the maximum level for Hg^{2+} ions concentration allowed by the U.S. Environmental Protection Agency (10 nM).

Reference:

1. H. Wang, Y. Wang, J. Jin and R. Yang, *Analytical Chemistry*, 2008, **80**, 9021-9028.
2. K. C. Grabar, R. G. Freeman, M. B. Hommer and M. J. Natan, *Analytical Chemistry*, 1995, **67**, 735-743.
3. S. Shinde, D.-Y. Kim, R. G. Saratale, A. Syed, F. Ameen and G. Ghodake, *Journal*, 2017, **7**.
4. S. Zhao, L. Chen, F. Liu, Y. Fan, Y. Liu, Y. Han, Y. Hu, J. Su and C. Song, *RSC Advances*, 2021, **11**, 30635-30645.
5. S. Siddiquee, S. Saallah, N. A. Bohari, G. Ringgit, J. Roslan, L. Naher and N. F. Hasan Nudin, *Journal*, 2021, **11**.
6. X. Liang, H. Wei, Z. Cui, J. Deng, Z. Zhang, X. You and X.-E. Zhang, *Analyst*, 2011, **136**, 179-183.
7. C.-Y. Lin, C.-J. Yu, Y.-H. Lin and W.-L. Tseng, *Analytical Chemistry*, 2010, **82**, 6830-6837.
8. J.-S. Lee, M. S. Han and C. A. Mirkin, *Angewandte Chemie International Edition*, 2007, **46**, 4093-4096.
9. P. An, H. Rao, M. Gao, X. Xue, X. Liu, X. Lu and Z. Xue, *Chemical Communications*, 2020, **56**, 9799-9802.
10. Y. Gao, X. Li, Y. Li, T. Li, Y. Zhao and A. Wu, *Chemical Communications*, 2014, **50**, 6447-6450.
11. M. Zhang, Y. Qu, D. Li, X. Liu, Y. Niu and Y. Xu, *Analytical Chemistry*, 2021, **93**, 10132-10140.